

# Switchless Multiplexing of Graphene Active Sensor Arrays for Brain Mapping

*Ramon Garcia-Cortadella<sup>†,∇</sup>, Nathan Schäfer<sup>†,∇</sup>, Jose Cisneros<sup>‡</sup>, Lucia Ré<sup>‡,§</sup>, Xavi Illa<sup>‡,§</sup>, Gerrit Schwesig<sup>||</sup>, Ana Moya<sup>‡</sup>, Sara Santiago<sup>⊥</sup>, Gonzalo Guirado<sup>⊥</sup>, Rosa Villa<sup>‡,§</sup>, Anton Sirota<sup>||</sup>, Francesc Serra-Graells<sup>‡</sup>, Jose A. Garrido<sup>†,§,\*</sup> and Anton Guimerà-Brunet<sup>‡,§,\*</sup>,*

<sup>†</sup> Catalan Institute of Nanoscience and Nanotechnology (ICN2), CSIC and BIST, Campus UAB, Bellaterra, 08193 Barcelona, Spain

<sup>‡</sup> Instituto de Microelectrónica de Barcelona, IMB-CNM (CSIC), Esfera UAB, Bellaterra, Spain

<sup>§</sup> Centro de Investigación Biomédica en Red en Bioingeniería, Biomateriales y Nanomedicina (CIBER-BBN), Madrid, Spain

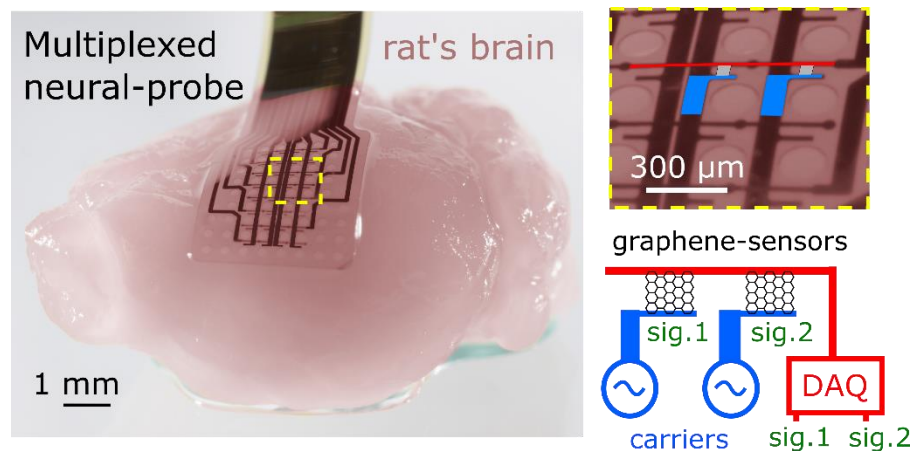
<sup>||</sup> Bernstein Center for Computational Neuroscience Munich, Munich Cluster of Systems Neurology (SyNergy), Faculty of Medicine, Ludwig-Maximilians Universität München, Planegg-Martinsried, Germany

<sup>⊥</sup> Departament de Química, Universitat Autònoma de Barcelona, 08193-Bellaterra, Barcelona, Spain

<sup>#</sup> ICREA, Pg. Lluís Companys 23, 08010 Barcelona, Spain

**ABSTRACT:** Sensor arrays used to detect electrophysiological signals from the brain are of major importance in neuroscience and biomedical engineering. However, the number of sensors that can be interfaced with macroscopic data acquisition systems currently limits the bandwidth of these devices. This bottleneck originates in the fact that, typically, sensors are addressed individually, requiring a connection for each of them. Herein, we present the concept of frequency-division multiplexing (FDM) of neural signals by graphene active sensors. We demonstrate the high performance of graphene transistors as mixers to perform amplitude modulation (AM) of neural signals *in-situ*, which is used to transmit multiple signals through a shared metal line. This technology eliminates the need for switches, remarkably simplifying the technical complexity of state-of-the-art multiplexed neural probes. Besides, the scalability of FDM graphene neural probes has been thoroughly evaluated and their sensitivity demonstrated *in-vivo*. Using this technology, we envision the implementation of a new generation of conformal neural probes with over a thousand channels for high bandwidth brain machine interfaces.

**GRAPHICAL TOC:**



**KEYWORDS:** Multiplexing, graphene, active sensors, bioelectronics, neural sensing

TEXT: Over the last decades, progress in neurotechnology has enabled a deeper understanding of brain functions such as motor control<sup>1,2</sup> or speech processing and synthesis<sup>3,4</sup>. In turn, these insights have prompted the realization of technological breakthroughs in the field of brain-computer interfaces (BCIs) such as partial restoration of movement<sup>5</sup> or decoding of speech from neural activity<sup>6</sup>. Cortical functions involved in such tasks often emerge from the integration of information in distinct brain regions, yet local activity from small groups of neurons carries essential information for neural coding<sup>7</sup>. Therefore, combining the coverage of large brain areas with high sensor density (i.e. high sensor count) is paramount for both neuroscientific and biomedical applications<sup>8-10</sup>. In this sense, one of the main limitations in current neurotechnologies originates in the need of individually connecting each sensing element to a signal amplifier. This constrain implies having as many conductive lines as sensors in the neural probes, which imposes a trade-off between sensor density and coverage area. One way to overcome this constrain is to perform multiplexing among sensors, which allows the transmission of multiple signals over a shared wire.

State-of-the-art sensing technologies for neuroscientific research are mostly based on intra-cortical electrode arrays<sup>11-14</sup>. Intra-cortical electrode arrays can be fabricated on rigid substrates<sup>15</sup>, therefore enabling to incorporate integrated-circuits on the probes<sup>12</sup> to amplify and multiplex the measured signals. However, intra-cortical probes cause serious tissue damage, limiting the mapping over large areas of the cortex, especially for biomedical applications. Alternatively, electrocorticography (ECoG) offers a minimally invasive way to acquire similar information<sup>16,17</sup>, by recording local field potentials<sup>18</sup> (LFP) from the surface of the brain. Nevertheless, planar  $\mu$ -ECoGs must be fabricated on a flexible substrate to provide conformability to the surface

morphology of the brain<sup>8,19</sup>. This constrain strongly limits the use of nanofabrication methodologies and available materials to fabricate integrated circuits on the neural probe, thus restricting the implementation of *in-situ* signal amplification for time-division multiplexing (TDM) of neural signals<sup>20</sup>. Flexible materials have been proposed to perform switching among active sensors in an addressable array configuration, including organic semiconductors<sup>21</sup> or ultra-thin silicon layers<sup>22</sup>. However, organic semiconductors present an insufficient mobility for high-speed operation, which is critical to achieve high sampling speed for large number of sensors, and the high complexity of ultra-thin silicon technology on flexible substrates limits its widespread application.

Herein, we present a novel approach that uses frequency-division multiplexing (FDM) of graphene solution-gated field-effect-transistors (g-SGFETs) in order to eliminate the need for on-site switches and to reduce the fabrication complexity of high-count neural probes. In this approach, neural signals detected by different graphene active sensors on the array are amplitude modulated (AM) by different carrier signals, allowing to transmit multiple signals through a shared communication channel. We present the fabrication of g-SGFET arrays on an addressable column/row matrix configuration to demonstrate their high performance for FDM operation *in-vivo*, sensing wide-band neural activity from the surface of the rat brain. Besides, we carefully assess the scalability of this technique, demonstrating its potential for simultaneously recording from over a thousand channels. The simplification of the technological complexity, achieved by the elimination of switches and the use of graphene electronics, opens the door to the implementation of high-count flexible neural probes as a readily available technology for neuroscientific studies as well as clinical applications.

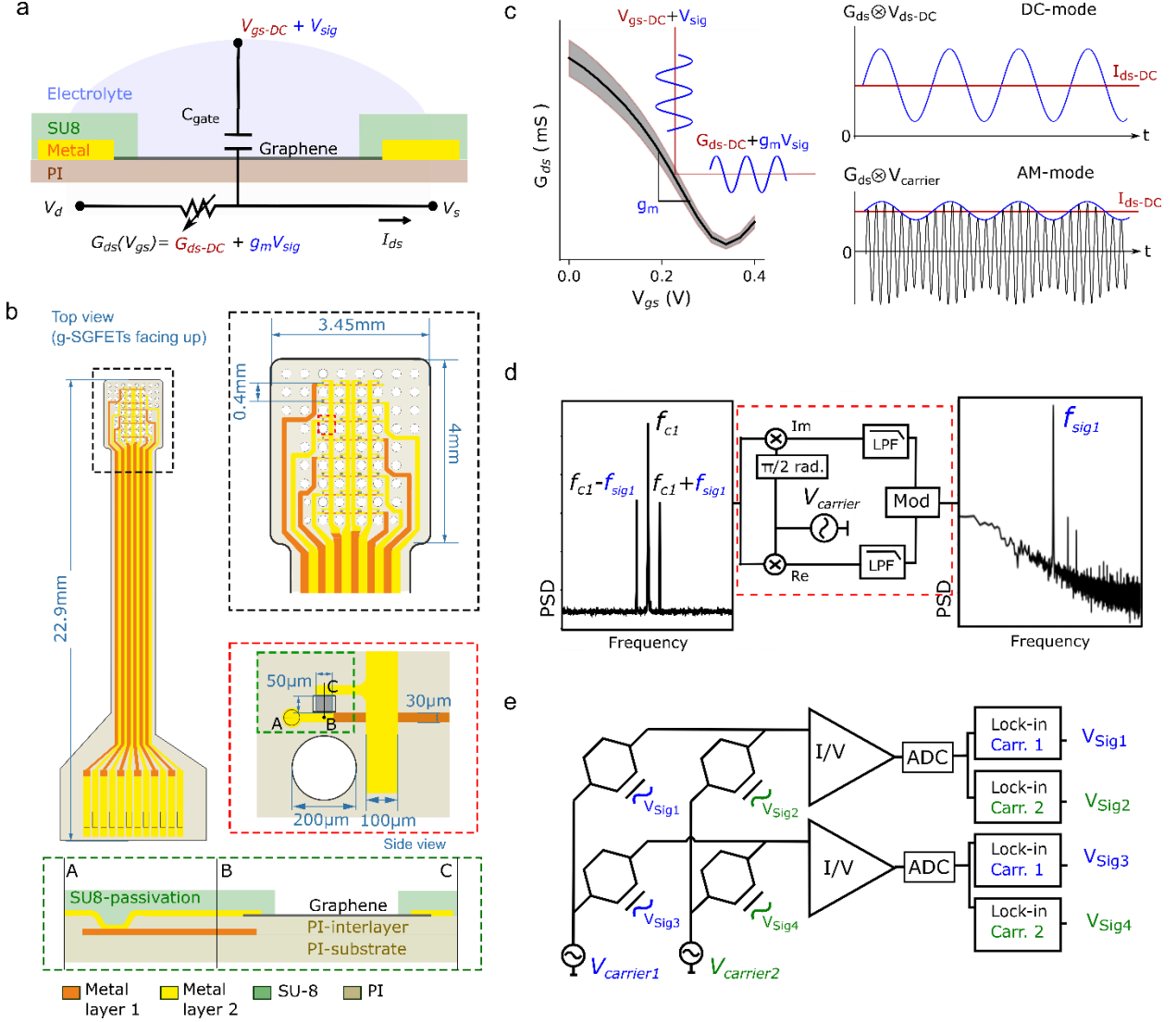


**Figure 1: Frequency-domain multiplexing of g-SGFET arrays:** **a.** Equivalent circuit of the g-SGFET together with an illustration of the device. **b.** Schematic of the neural probe layout. On the left, the whole probe is displayed. A zoom into the probe tip is shown on the top-right image. The orange/yellow colour represent the 1<sup>st</sup>/2<sup>nd</sup> metal layers, separated by a 2μm thick polyimide layer. A zoom into a single pixel is shown within the red dashed-line square. The bottom schematic depicts a side view of the g-SGFET, showing the connection between the 1<sup>st</sup> and 2<sup>nd</sup> metal layer through a VIA hole in the PI. **c.** Typical  $G_{ds} - V_{gs}$  curve of g-SGFETs. The filled area represents the standard deviation ( $n = 8$ ). The definition of normalized transconductance ( $g_m$ ) as the slope of

the  $G_{ds} - V_{gs}$  curve, is indicated in the graph. The g-SGFETs acts as a multiplier of the drain-to-source voltage and the signal at the gate. The resulting  $I_{ds}$  in the DC and AM modes is illustrated.

**d.** The signal folded by the carrier is shown in the frequency domain (left). Demodulation scheme (middle): the multiplication of the modulated signal by an oscillator at the carrier frequency of interest and the  $\pi/2$  radians phase shifted oscillator allows to recover the module of the signal in the baseband (right). **e.** Basic schematic of the addressable g-SGFET array, which allows modulating the signals at the gate of different g-SGFETs with different carrier frequencies. The mixed signals, containing multiple carrier frequencies, are demodulated after current-to-voltage conversion and digitalization.

## FREQUENCY-DIVISION MULTIPLEXING OF G-SGFET ARRAYS

G-SGFETs have been proposed as signal transducers in the field of biosensing and bioelectronics<sup>19,23–25</sup>, presenting unique properties for the detection of full-band neural signals, from infra-slow to high-frequency components, with a high spatial resolution<sup>26</sup>. Besides, as active sensors, G-SGFETs provide an intrinsic pre-amplification of the signal and can be arranged in a column/row addressable matrix due to their two terminal (i.e. drain and source) configuration (see Fig. 1a and 1b). These properties, combined with their remarkable frequency response<sup>27</sup>, make g-SGFETs an ideal technology for the implementation of frequency-division sensor arrays.

In g-SGFETs, the graphene channel is placed in contact with an electrolyte gate, i.e. the brain tissue in the case of neural sensing applications. Electrical potential fluctuations in the environment influence the conductivity of the transistor channel through the gate capacitance. The constant of proportionality between drain-source conductance ( $G_{ds}$ ) and the electrical potential at

the interface ( $V_{gs}$ ) is referred to as the transconductance<sup>28</sup> ( $g_m$ ). g-SGFETs can be modelled by the equivalent circuit shown in Fig. 1a. Its stationary response to a constant bias ( $V_{gs-DC}$ ) is described by the voltage dependent term  $G_{ds-DC}$ , while its dynamic response to a small-amplitude, time-dependent signal ( $V_{sig}$ ) is characterised by the term  $V_{sig}g_m$ . In the typical operation mode (DC mode), the drain-source bias  $V_{ds}$  is constant; thus, the only time variations in the drain-source current ( $I_{ds}$ ) are caused by variations in  $G_{ds}$  (Fig. 1c). On the other hand, in FDM (or amplitude modulation- AM mode), the drain-source bias is typically a pure tone signal ( $V_{carrier}(t)$ ). Therefore,  $I_{ds}$  results from the product of  $V_{carrier}(t)(g_m V_{sig}(t) + G_{ds-DC})$  (see Fig. 1c).

The multiplication of  $V_{carrier}$  and  $V_{sig}$  produces the folding of their frequencies. In the frequency-domain representation of  $V_{carrier}(t) * V_{sig}(t)$  (Fig. 1d-left), a peak at the carrier frequency ( $f_c$ ) can be observed, which is proportional to  $G_{ds-DC}$ . In addition, two side bands (at  $f_c - f_{sig}$  and  $f_c + f_{sig}$ ) appear, the amplitude of which is proportional  $g_m V_{sig}$ . This mixed signal can then be demodulated by a lock-in amplifier (see Fig. 1d-middle) producing the folding of the side bands back to the baseband frequency (see Fig. 1d-right), with the DC-offset corresponding to the stationary component of  $I_{ds}$ . This demodulation can be repeated for different carrier frequencies to recover the neural signals detected in each of the graphene sensors. The schematic in Fig. 1e represents the FDM of a 2x2 sensor array. Carrier signals with different frequencies ( $f_c$ ) are applied at each column of the array and independent data-acquisition channels are connected to each of the drains to reliably recover the information from the multiplexed sensors. Here, we present frequency-division multiplexed arrays of up to 4x8 graphene sensors fabricated on a flexible polyimide (PI) substrate (see Fig. 1b and supporting information for more details of the fabrication method). For the characterization of the FDM sensor arrays and their operation *in-vivo*,

we have developed a recording system based on a PXIe for high sampling speed and a custom built front-end amplifier for current-voltage conversion (see supporting information).

## ***IN-VITRO* CHARACTERIZATION OF FDM GRAPHENE NEURAL PROBES**

In order to validate the suitability of g-SGFETs for frequency-division multiplexing, their sensitivity in the AM mode must be characterized and compared with the sensitivity in the DC mode. The characterization of  $g_m$  can be performed following two approaches: from the derivative of the stationary  $G_{ds} - V_{gs}$  curve or from the dynamic response of g-SGFETs to signals with various frequency components applied at the gate (see Fig. 1c). Fig. 2a shows the  $g_m - V_{gs}$  curves extracted following the first approach for a 3x3 g-SGFET array, demonstrating the equivalence of the stationary response in the DC and AM operation modes. Fig. 2b presents the frequency dependence of  $g_m$  measured following the second approach. The magnitude of  $g_m$  presents similar values in both modes for frequencies  $< 1kHz$ , above which the effect of capacitive currents contributes significantly in the DC mode (see supporting information). In addition to the transconductance, the intrinsic electrical noise of the graphene transistors shall be considered in order to fully characterise the sensitivity of the graphene sensors. In Fig. 2c, the equivalent noise at the gate ( $V_{gs-rms}$ ), defined as the RMS current noise ( $I_{ds-rms}$ ) normalized by the transconductance, is represented under different  $V_{gs}$  bias conditions for a transistor area of  $50\mu m \times 50\mu m$ . Fig. 2c demonstrates that the sensitivity of g-SGFETs, defined by their noise performance, does not differ dramatically in both modes, showing only slight changes in its  $V_{gs}$  dependence.



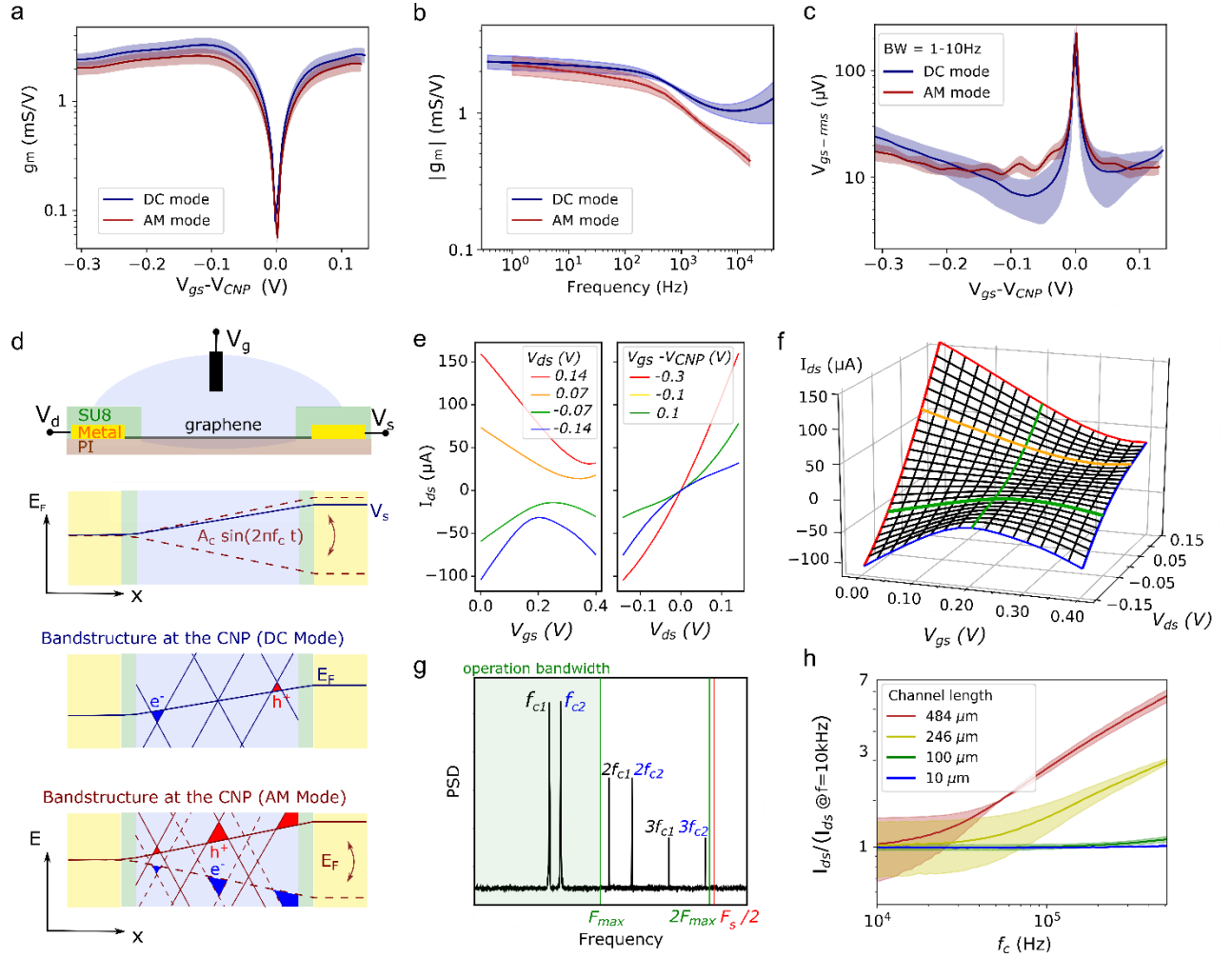


**Figure 2| In-vitro evaluation of g-SGFET performance in the amplitude modulation (AM) mode.** **a.**  $g_m - V_{gs}$  relationship in the AM and DC modes, measured in a 3x3 g-SGFET array. **b.** The magnitude of  $g_m$  over frequency of the signal applied at the gate is shown for the two modes. The response was measured in a 2x2 g-SGFET array. **c.**  $V_{gs-rms}$  for an integration bandwidth of 1-10Hz measured in the AM and DC modes; measurements performed with a 3x3 g-SGFET array. **d.** Schematic representation of a g-SGFET and the Fermi energy in the graphene for the DC and AM mode (top). The band structure at the CNP point is shown along the graphene channel for the DC (middle) and AM (bottom) modes. **e.** Dependence of  $I_{ds}$  on  $V_{gs}$  and  $V_{ds}$ , revealing the shift in the CNP, as well as the non-linearities in the  $I_{ds} - V_{ds}$  produced by the effective gating. **f.** 3-

dimensional representation of the  $I_{ds}$  dependence on  $V_{gs}$  and  $V_{ds}$ . The relation between shifts of  $I_{ds} - V_{gs}$  along the  $V_{gs}$  axis and non-linearities introduced in the  $I_{ds} - V_{ds}$  curves can be observed. **g.** Two carrier signals and their 2<sup>nd</sup> and 3<sup>rd</sup> order harmonics are represented in the frequency domain. The frequency which defines the bandwidth of operation ( $F_{max}$ ) and the position of the Nyquist frequency ( $F_s/2$ ) with respect to  $F_{max}$  are indicated by the vertical lines. **h.** The  $I_{ds}$  normalized by its value at 10kHz is shown for different channel lengths. The filled area represents the standard deviation (n=3).

These slight discrepancies presumably arise from the differences in the drain-source bias in both modes. The gradient in the workfunction of graphene along the channel induced by this bias causes a non-homogeneous effective gating of the transistor (see Fig. 2d and supporting information). In the DC mode this gradient is constant over time, producing a constant offset in the channel doping for a certain  $V_{ds}$  bias. Changing  $V_{ds}$  produces a shift of the transfer curves of the g-SGFETs along the  $V_{gs}$  axis (see Fig. 2e). This effective gating is also responsible for the dependence of  $G_{ds}$  on  $V_{ds}$ , which introduces non-linearities in the output characteristics shown in Fig. 2e. Fig. 2f shows a 3-dimensional representation of the  $I_{ds} - V_{gs}$  and  $I_{ds} - V_{ds}$  characteristic curves of the g-SGFETs. In the DC mode, the g-SGFETs are operated at a stationary point in the  $V_{gs} - V_{ds}$  plane, but in the AM mode the drain-source bias oscillates along the  $V_{ds}$  axis. In this way, non-linearities in the  $I_{ds} - V_{ds}$  curves will lead to distortion of the carrier signal, introducing harmonics at frequencies multiple of  $f_c$  (see Fig. 2g and supporting information). Harmonic distortion constrains the selection of carrier frequencies that can be used for AM: high order harmonics must not lie within the frequency band of operation dedicated to the carrier signals.

Thereby, the frequency of all carriers must be below the 2<sup>nd</sup> order harmonic of the carrier of lowest frequency (see Fig. 2g). In addition, the Nyquist frequency ( $f_s/2$ ) must be above the 2<sup>nd</sup> order harmonic of the highest carrier frequency in order to prevent folding of 3<sup>rd</sup> order harmonics into the band of operation by aliasing.

Another important aspect affecting the selection of carrier frequencies is the frequency response of g-SGFETs. The graphene-electrolyte interface exhibits a capacitive response, which at high frequencies allows a displacement current to flow from drain to source through the electrolyte<sup>27</sup>, degrading the device performance. The characteristic cut-off frequency of this phenomenon appears at relatively high frequencies due to the high ratio between mobility and interface capacitance in graphene. Other active sensors, such as organic electrochemical transistors, which present a lower mobility and a larger interface capacitance<sup>29</sup>, are expected to present a worse frequency response<sup>27</sup>. Fig. 4e shows the frequency response of g-SGFETs for multiple channel lengths, demonstrating an approximately constant response for channels shorter than  $100\mu m$  and frequencies below  $500kHz$  at least.

## SCALABILITY OF FDM GRAPHENE NEURAL PROBES

Considering the ultimate goal of enabling high-density, large-area sensor arrays, the scalability of the FDM graphene neural probes has to be thoroughly explored. Important aspects limiting the scalability of FDM are the crosstalk in the g-SGFET array, the constraints in the selection of carrier frequencies, and the requirements for the electronics used to operate the arrays.

In FDM, no switching among sensing sites is required. Although this feature bears a clear advantage for ease of fabrication of the neural probes, it prevents from doing on-site switching of

the sensors, and can therefore lead to an increased susceptibility to crosstalk. Crosstalk can appear between g-SGFETs in the same row (i.e. sharing a readout channel) as well as in the same column (i.e. biased by the same carrier) due to common-mode voltage ( $V_{com}$ ) oscillations in the resistance of metal tracks in series with the drain ( $R_{row}$ ) and source ( $R_{col}$ ). Analysing the equivalent circuit in Fig. 3a, an analytical expression can be derived, which indicates that crosstalk among rows and among columns is proportional to  $R_{row}$  and  $R_{col}$  respectively (see Fig. 3a and supporting information). Additionally, crosstalk signals couple with g-SGFETs that are out of the same column and row, causing a second order crosstalk (see supporting information S4). In order to experimentally determine the crosstalk level, we have patterned multiple polyelectrolyte gates on the graphene sensor arrays by inkjet printing (see Fig. 3a and supporting information S5). Fig. 3b shows the signal measured by an individually gated g-SGFET (black) and the crosstalk it induced on sensors in the same column (orange), the same row (blue) and on the rest of g-SGFETs (red), together with the fitting of the experimental data using the analytical expression presented in the supporting information. A crosstalk of  $\sim 36\text{dB}/\sim 73\text{dB}$  is observed for g-SGFETs within/outside the same column or row, which corresponds to a  $R_{row} \approx R_{col} = 50\Omega$ . In order to reduce the crosstalk to the level achieved using on-site switches ( $\sim 65\text{dB}$ )<sup>30</sup>, the resistance of the tracks should be reduced to the range of few ohms. This target could be met by increasing the width of the metal lines, which can be implemented easily when translating this technology from rodents research into human clinical applications. .

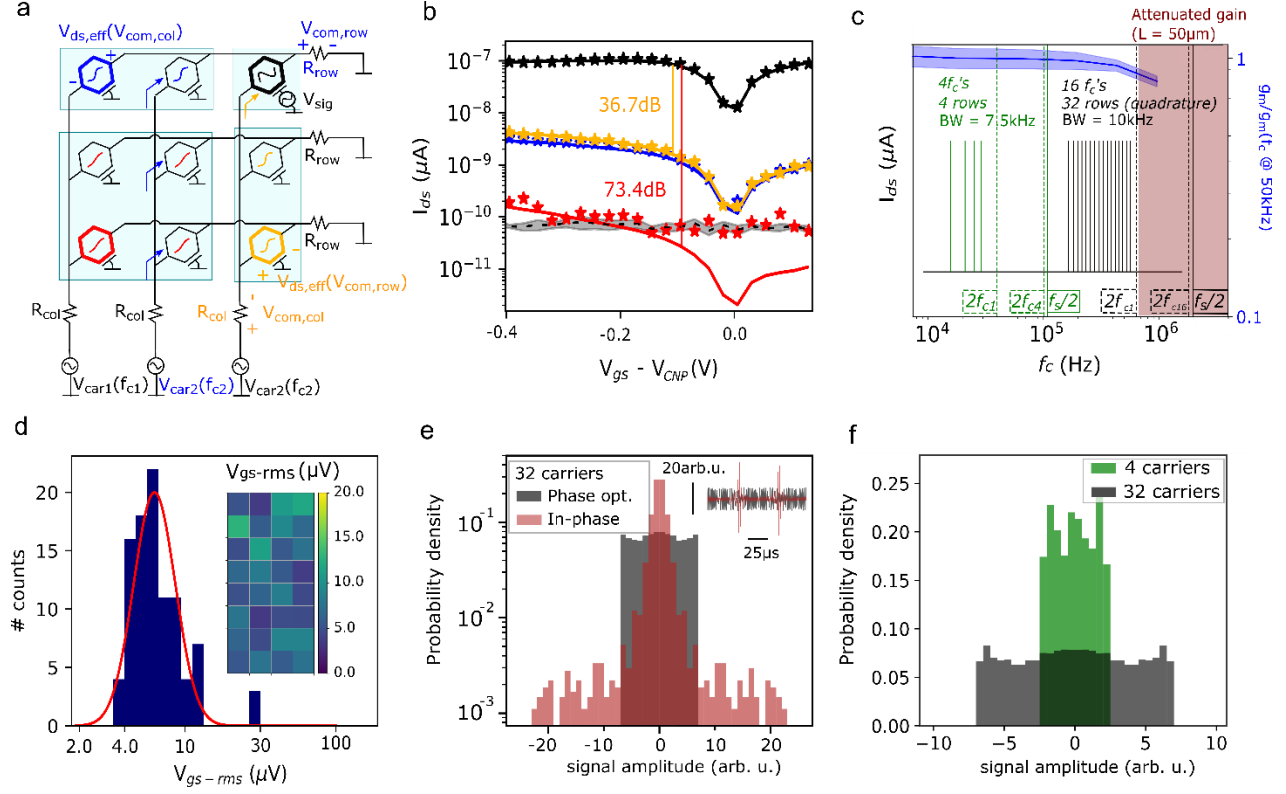


**Figure 4| Scalability of g-SGFET arrays multiplexed in the frequency-domain: a.** Equivalent circuit of a 3x3 g-SGFET array. The metal track resistance of the columns and rows is modelled by  $R_{col}$  and  $R_{row}$  respectively. Each column is biased with a different carrier ( $V_{car1}$ ,  $V_{car2}$  and  $V_{car3}$ ). Common voltage oscillations ( $V_{com,col}$  and  $V_{com,row}$ ) produce changes in  $V_{ds,eff}$ . The light blue area indicates the position of 4 polyelectrolyte gates printed on a 3x3 array. **b.** Response to a 10Hz signal measured in the g-SGFETs highlighted by a thicker colored line in part **a**. The solid lines indicate the fitting by the analytical model. The noise (dashed black line) was measured at 7Hz. **c.** The right axis indicates the normalized transconductance for g-SGFETs of ( $50\mu m \times 50\mu m$ ,  $n=4$ ). The carrier frequencies selected for the *in-vivo* proof of concept (4x8 array) are shown in green and those proposed for a 32x32 sensor array are indicated in black. High order harmonics are indicated together with the required sampling frequency. **d.** Histograms of  $V_{gs-rms}$  from 3 neural probes of 32 g-SGFETs integrated in the 1-10Hz frequency. The log-normal

distribution indicates the mean and standard deviation of  $V_{gs-rms}$ . The values from the specific neural probe which was implanted in shown in the inset figure. **e.** Histogram of 32 superposed carriers with phase optimization to minimize the peak-to-peak amplitude (black), and with all carriers in phase (red). The inset shows a fragment of the resulting signals. **f.** Histogram of the 4 superposed carriers used for the *in-vivo* proof of concept compared to the amplitude of a 32-carrier signal with phase optimization.

Another important aspect related to the scalability of FDM graphene neural probes is the selection of the carrier frequencies, which is constrained by the frequency response of g-SGFETs and the harmonic distortion of the carrier signals. The  $g_m(f_c)$  was characterized by sweeping  $f_c$  and measuring the dynamic response of the graphene sensors to pure tone signals applied at the gate. Fig. 3c shows that  $g_m$  remains approximately constant for carrier frequencies up to at least 600kHz and a channel length of 50 $\mu m$ . Sampling at four times this frequency limit (i.e.  $F_s/2 \geq 2F_{max} = 1.2 MHz$ ) allows to use carriers of up to  $\sim 600kHz$ . Fig. 3c shows a combination of carrier frequencies which meets all the requirements to allow the operation of 32x32 graphene sensor arrays. In this configuration, operation in quadrature AM<sup>31</sup> can be used to maximize the frequency bandwidth of each sensor to 10kHz (see Fig. 3c). Above this bandwidth, the signal will be filtered in the digital domain to eliminate any components corresponding to other carriers.

The discrete electronics system designed for the validation of the technology *in-vivo* is limited to operate arrays of up to 4x8 g-SGFETs. This limitation comes from the constrained scalability of discrete electronics, in opposition to application specific integrated circuits (ASIC). Fig. 3c shows the combination of carrier frequencies used for the *in-vivo* proof of concept. The  $V_{gs-rms}$  from 3 probes of 4x8 g-SGFET arrays operated with this carriers configuration is shown in Fig. 3d, demonstrating a mean sensitivity of 6.29 $\mu V$  with a standard deviation of 1.37  $\mu V$  and

a yield of 100%. This high sensitivity can eventually degrade due to the superposition of a large number of carrier signals, the large amplitude of which might challenge the resolution of the data acquisition (DAQ) system. The quantization error of the analog-to-digital converter (ADC), given by its less-significant bit (LSB), must be low enough to ensure signal integrity. When increasing the number of carriers, their amplitude ( $A_c$ ) must be reduced in order to prevent saturation of the ADC (see supporting information). This decrease in  $A_c$  implies an attenuation of the transconductance (i.e.  $A_c g_m$ ) of the g-SGFETs, while the LSB of the ADC remains unchanged. To minimize the amplitude of the carriers superposition for a certain  $A_c$ , the phase of the carriers can be adjusted. Fig. 3e shows the improvement obtained by phase optimization for the combination of 32 carrier signals defined in Fig. 3c, revealing a threefold attenuation in the amplitude of the carrier superposition. The comparison with the superposition of the 4 carriers used for this proof of concept shows that upscaling to 32 carriers causes an increase in the amplitude by a factor of 2.8, which could be compensated by increasing the resolution of the ADC by 1-2 bits<sup>32</sup>. These results, together with the measure of crosstalk and the high frequency response of g-SGFETs, demonstrate the potential of this technology to reach over a thousand channels flexible neural probes.

## ***IN-VIVO* EVALUATION OF FDM GRAPHENE NEURAL PROBES**

Previous works have shown that g-SGFETs operated in the DC mode present a high sensitivity for the recording of neural activity<sup>19,23</sup>. Moreover, g-SGFETs have demonstrated a unique capability for the recording of infra-slow neural activity with a high spatial resolution<sup>26</sup>. The FDM operation of g-SGFETs is not only expected to preserve their sensitivity for infra-slow signals, but to enhance their performance by eliminating flicker noise from the amplifiers due to the lock-in amplification in the AM mode. To validate the *in-vivo* functionality of FDM graphene

probes, we have recorded electrical activity from the cortex of a Long Evans rat in an acute setting using a 4x8 FDM graphene neural probe (see Fig. 4a-b and supporting information). The optimum  $V_{gs}$  which maximizes  $g_m$  and the highest carriers amplitude ( $A_c$ ), which fills the dynamic range of the amplifiers were determined *in-vivo* (see Fig. 4c).

The sensitivity of the sensors to high-frequency LFP activity was evaluated by measuring visually evoked potentials<sup>33</sup> triggered by a blue LED emitting light-pulses of 100 ms every 5s. The sensors directly placed on the primary visual cortex V1 (lower left) exhibit a sharp response with 50 ms delay and 250  $\mu$ V peak amplitude lasting until 100 ms after the initial trigger (Fig. 4d). Sensors placed further away from the V1 show a distance-dependent suppressed response of smaller amplitude and extended delay (Fig. 4e). This result is in full agreement with previously reported values<sup>33</sup>, demonstrating the preserved sensitivity of g-SGFETs in this frequency band in the FDM operation mode.

Similarly, the distortion-free recording of infra-slow activity using g-SGFET has been previously shown in the DC mode by the recording of cortical spreading depression (CSD) events<sup>26</sup>. CSDs are a slowly propagating wave of depolarizing neurons and astrocytes, which has been clinically related to stroke, brain injury and migraine<sup>34,35</sup>. CSDs can be easily triggered by injecting KCl into the brain cortex and present a propagation speed of approximately 5 mm per minute across the cortex. Fig. 4f shows the spontaneous activity under anaesthesia where highly coherent transitions from up to down-states can be observed. Fig. 4g shows the signal from channel in position (1,5) filtered in the 1-50Hz frequency band (blue) together with the signal filtered in the 0.001-50Hz band. This spontaneous activity is strongly suppressed during the depolarization wave, which results in a large infra-slow signal drift with a duration over 70s. Fig. 3h shows the propagating front of the CSD wave across the array, demonstrating the capabilities



of FDM graphene neural probes to study topography of wide-band oscillatory dynamics in the brain.

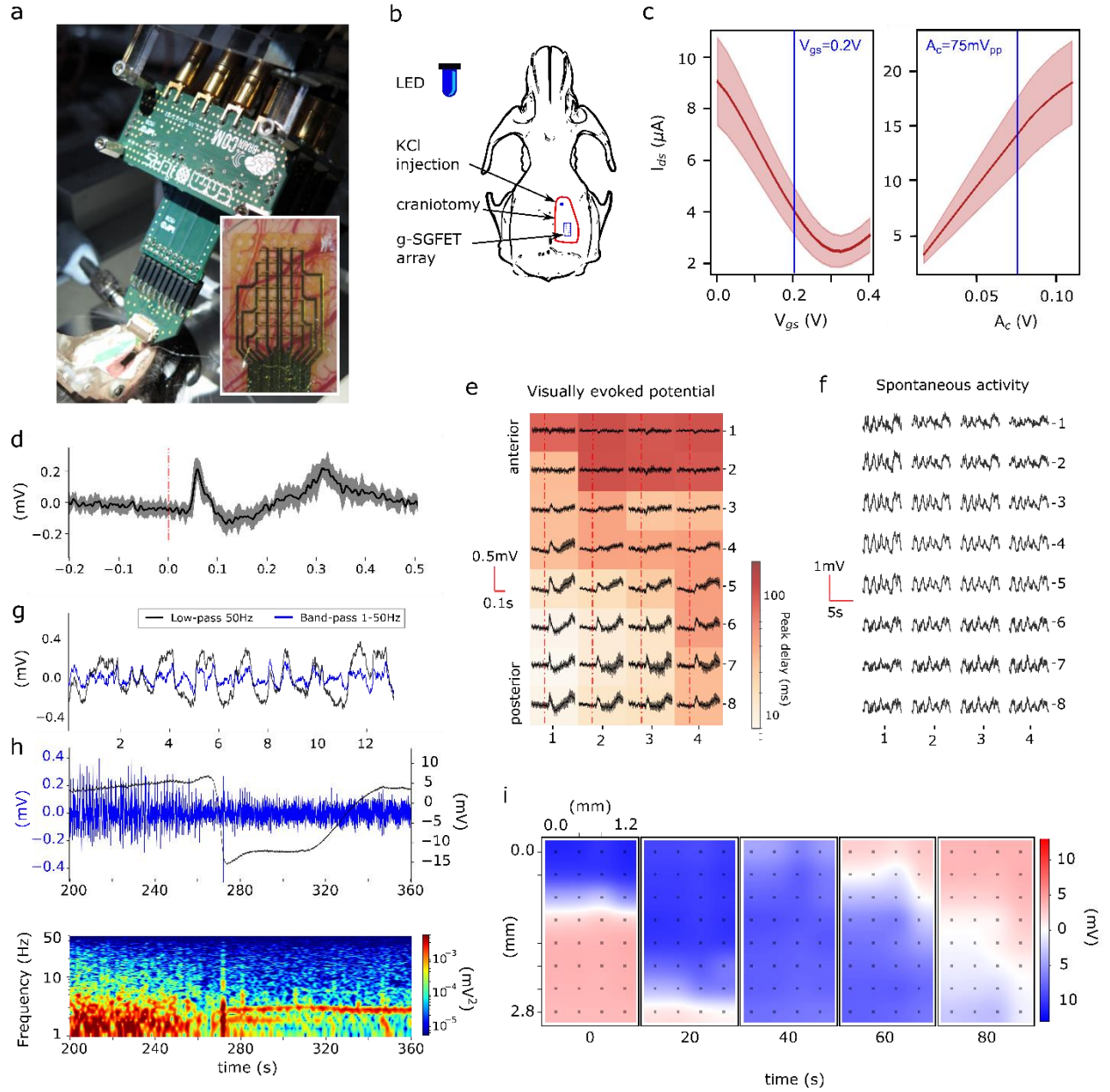


**Figure 3| In vivo validation of FDM graphene neural probes for brain recordings: a.** Acute experiment setting. The g-SGFET array interfaces the brain with the custom-built front-end amplifier. **b.** Illustration of a rat skull indicates the position of the craniotomy, the g-SGFET array, the LED and the place of KCl injection. **c.** Average and standard deviation of the  $I_{ds} - V_{gs}$  and  $I_{ds} - A_c$  curves obtained *in-vivo* for the 32 channels. **d.** The visually evoked potential averaged

over 10 consecutive events is shown for the g-SGFET placed on the lower-left corner of the array. **e.** Visually evoked potential averaged over 10 consecutive events for all g-SGFETs on the 4x8 array. The colour map represents the delay between stimulus and the peak of the response. **f.** Map of spontaneous activity under anaesthesia. **g.** Spontaneous activity filtered in two different bands indicates the presence of low frequency components ( $< 1\text{Hz}$ ) for channel in position (1,5). **h.** CSD event recorded in a single g-SGFET. The top graph shows the activity in the 1-50Hz band (blue, left axis) and the wide-band activity (0.001 – 50Hz) (black, right axis). The corresponding spectrogram in the 1-50Hz band is shown below. **i.** The colour maps indicate the signal amplitude in each of the g-SGFETs on the array at different times during the CSD propagation.

## Discussion

In summary, we have presented the concept of frequency-division multiplexing of graphene active sensor arrays to reduce the number of wires required for high sensor-count neural probes. This novel approach presents two main advantages over time-division multiplexing resulting from its switchless operation. Firstly, the elimination of switches implies an enormous simplification of the technological complexity, eliminating the need for high-mobility and wide band-gap flexible materials, such as ultra-thin  $\text{SiO}_2$ . Secondly, FDM operates in a continuous mode, fully circumventing the problems derived from limited switching speed and artefacts in TDM, which ultimately limit the scalability of the arrays. Moreover, the signals from all sensors are continuously sampled at high speed, in the MHz range. Although the frequency separation between carriers determines the bandwidth of the sensors, the high sampling speed allows to acquire the neural signals with an arbitrarily high oversampling. Finally, the modulation and subsequent demodulation of the signals in the FDM mode is based on a lock-in amplification

scheme, which eliminates flicker noise from the amplifiers and improves the sensitivity of the system in the infra-slow frequency band.

Our results demonstrate the high performance of g-SGFETs as mixers to perform on-site amplitude modulation of neural signals. We have shown their high sensitivity for wide-band neural signals both in the beaker as well as *in-vivo*. Besides, we have also demonstrated the outstanding drain-source frequency response of solution-gated graphene sensors, validating their performance for high carrier frequencies, required for the operation of large-scale arrays. In addition, we have evaluated the crosstalk among sensing sites, which could reach the same level as for TDM with on-site switches when translating this technology to human scale neural probes. In order to maintain the sensitivity of the system for large arrays, with up to 32 superposed carriers, we have described the use of carrier phase optimization as well as the requirements for the DAQ system, which could be met by an ASIC<sup>32</sup>.

The viability of large arrays controlled by an ASIC allows to envision the realization of a new generation of high-density and large-area sensor arrays with thousands of sensing sites. The simplicity and robustness of the switchless, FDM methodology compared to state of the art alternatives<sup>30,36</sup>, together with the high sensitivity, flexibility and biocompatibility of graphene active sensors make the implementation of these technologies very promising for both neuroscientific research as well as clinical applications.

## ASSOCIATED CONTENT

### Supporting Information.

Fabrication process of the graphene sensor arrays. Electrical setup hardware and software for device characterization and *in-vivo* proof of concept. Animal handling and device implantation. High frequency response in DC-mode. Non-homogeneous doping of graphene transistors. Carriers and baseband harmonic distortion. Crosstalk modelling. DAQ noise. (PDF)

## AUTHOR INFORMATION

### Corresponding Author

\* [joseantonio.garrido@icn2.cat](mailto:joseantonio.garrido@icn2.cat) (Jose A. Garrido) and [anton.guimera@imb-cnm.csic.es](mailto:anton.guimera@imb-cnm.csic.es) (Anton Guimerà Brunet)

### Author Contributions

R.G.C. Contributed to the design and fabrication of the neural sensor arrays. He characterized the devices and contributed to the software development and *in-vivo* experiments. N.S. Contributed to the design of the sensor arrays, DAQ system design and *in-vivo* experiments. J.C. Designed the front-end and contributed to the characterization of the DAQ system. L.R. Contributed to the software development and devices characterization. X.I. Contributed to the design and fabrication of the neural sensor arrays. G.S. Did the surgery for the acute experiment. A.M. Developed the inkjet printing procedure to evaluate the crosstalk. S.S. and G.G. Developed the polyelectrolytes used for crosstalk determination. A.S. Led the team for the *in-vivo* proof of concept. F.S.G. Contributed to the concept of frequency-division multiplexing of graphene sensor arrays and the design of the front-end. R.V. Provided support for the development of the software and hardware.

A.G.B. Contributed to the experimental design, development of the software and hardware as well as *in-vivo* proof of concept. J.A.G. Led the team for development of the graphene sensor arrays and contributed to the experimental design. R.G.C., A.G.B. and J.A.G. wrote the manuscript.

<sup>▽</sup> R.G.C. and N.S contributed equally to this work.

## Notes

Patent application (no. EP18382593) filled by UAB, CSIC and ICN2; entitled “Circuit for the multiplexing and read-out of variable-resistance sensor arrays” (pending); inventors who are co-authors in the present article are AGB, FSG and JAG.

## ACKNOWLEDGMENT

This work has been funded by the European Union’s Horizon 2020 research and innovation programme under Grant Agreement No. 732032 (BrainCom) and Grant Agreement No 785219 (Graphene Flagship). The ICN2 is supported by the Severo Ochoa Centres of Excellence programme, funded by the Spanish Research Agency (AEI, grant no. SEV-2017-0706), and by the CERCA Programme / Generalitat de Catalunya. R.G.C. and N.S. acknowledge that this work has been done in the framework of the PhD in Electrical and Telecommunication Engineering at the Universitat Autònoma de Barcelona. R.G.C is supported by the International PhD Programme La Caixa - Severo Ochoa (Programa Internacional de Becas "la Caixa"-Severo Ochoa). This work has made use of the Spanish ICTS Network MICRONANOFABS partially supported by MICINN and the ICTS ‘NANBIOSIS’, more specifically by the Micro-NanoTechnology Unit of the CIBER in Bioengineering, Biomaterials and Nanomedicine (CIBER-BBN) at the IMB-CNM. This work is within the project FIS2017-85787-R funded by the “Ministerio de Ciencia, Innovación y

Universidades” of Spain, the “Agencia Estatal de Investigación (AEI)” and the “Fondo Europeo de Desarrollo Regional (FEDER/UE)”.

#### REFERENCES:

- (1) Jeannerod, M. *Motor Cognition : What Actions Tell the Self*; Oxford University Press, 2006.
- (2) Georgopoulos, A. P.; Kettner, R. E.; Schwartz, A. B. Primate Motor Cortex and Free Arm Movements to Visual Targets in Three-Dimensional Space. II. Coding of the Direction of Movement by a Neuronal Population. *J. Neurosci.* **1988**, 8 (8), 2928–2937.
- (3) Wilson, S. M.; Saygin, A. P.; Sereno, M. I.; Iacoboni, M. Listening to Speech Activates Motor Areas Involved in Speech Production. *Nat. Neurosci.* **2004**, 7 (7), 701–702. <https://doi.org/10.1038/nn1263>.
- (4) Galantucci, B.; Fowler, C. A.; Turvey, M. T. The Motor Theory of Speech Perception Reviewed. *Psychon. Bull. Rev.* **2006**, 13 (3), 361–377. <https://doi.org/10.3758/BF03193857>.
- (5) Capogrosso, M.; Milekovic, T.; Borton, D.; Wagner, F.; Moraud, E. M.; Mignardot, J.-B.; Buse, N.; Gandar, J.; Barraud, Q.; Xing, D.; et al. A Brain–Spine Interface Alleviating Gait Deficits after Spinal Cord Injury in Primates. *Nature* **2016**, 539 (7628), 284–288. <https://doi.org/10.1038/nature20118>.
- (6) Anumanchipalli, G. K.; Chartier, J.; Chang, E. F. Speech Synthesis from Neural Decoding of Spoken Sentences. *Nature* **2019**, 568 (7753), 493–498. <https://doi.org/10.1038/s41586-019-1119-1>.
- (7) Averbeck, B. B.; Latham, P. E.; Pouget, A. Neural Correlations, Population Coding and

- Computation. *Nat. Rev. Neurosci.* **2006**, 7 (5), 358–366. <https://doi.org/10.1038/nrn1888>.
- (8) Khodagholy, D.; Gelinas, J. N.; Thesen, T.; Doyle, W.; Devinsky, O.; Malliaras, G. G.; Buzsáki, G. NeuroGrid: Recording Action Potentials from the Surface of the Brain. *Nat. Neurosci.* **2015**, 18 (2), 310–315. <https://doi.org/10.1038/nn.3905>.
  - (9) Chang, E. F. Towards Large-Scale, Human-Based, Mesoscopic Neurotechnologies. *Neuron* **2015**, 86 (1), 68–78. <https://doi.org/10.1016/j.neuron.2015.03.037>.
  - (10) Stringer, C.; Pachitariu, M.; Steinmetz, N.; Reddy, C. B.; Carandini, M.; Harris, K. D. Spontaneous Behaviors Drive Multidimensional, Brainwide Activity. *Science* (80-. ). **2019**, 364 (6437), eaav7893. <https://doi.org/10.1126/SCIENCE.AAV7893>.
  - (11) Chung, J. E.; Joo, H. R.; Fan, J. L.; Liu, D. F.; Barnett, A. H.; Chen, S.; Geaghan-Breiner, C.; Karlsson, M. P.; Karlsson, M.; Lee, K. Y.; et al. High-Density, Long-Lasting, and Multi-Region Electrophysiological Recordings Using Polymer Electrode Arrays. *Neuron* **2019**, 101 (1), 21-31.e5. <https://doi.org/10.1016/J.NEURON.2018.11.002>.
  - (12) Jun, J. J.; Steinmetz, N. A.; Siegle, J. H.; Denman, D. J.; Bauza, M.; Barbarits, B.; Lee, A. K.; Anastassiou, C. A.; Andrei, A.; Aydın, Ç.; et al. Fully Integrated Silicon Probes for High-Density Recording of Neural Activity. *Nature* **2017**, 551 (7679), 232–236. <https://doi.org/10.1038/nature24636>.
  - (13) Ferro, M. D.; Proctor, C. M.; Gonzalez, A.; Zhao, E.; Slezia, A.; Pas, J.; Dijk, G.; Donahue, M. J.; Williamson, A.; Malliaras, G. G.; et al. NeuroRoots, a Bio-Inspired, Seamless Brain Machine Interface Device for Long-Term Recording. *bioRxiv* **2018**, 460949. <https://doi.org/10.1101/460949>.
  - (14) Musk, E.; Neuralink. An Integrated Brain-Machine Interface Platform with Thousands of Channels. *bioRxiv* **2019**, 703801. <https://doi.org/10.1101/703801>.

- (15) Kook, G.; Lee, S. W.; Lee, H. C.; Cho, I.-J.; Lee, H. J. Neural Probes for Chronic Applications. *Micromachines* **2016**, 7 (10). <https://doi.org/10.3390/mi7100179>.
- (16) Chao. Long-Term Asynchronous Decoding of Arm Motion Using Electrographic Signals in Monkey. *Front. Neuroeng.* **2010**. <https://doi.org/10.3389/fneng.2010.00003>.
- (17) Yeager, J. D.; Phillips, D. J.; Rector, D. M.; Bahr, D. F. Characterization of Flexible ECoG Electrode Arrays for Chronic Recording in Awake Rats. *J. Neurosci. Methods* **2008**, 173 (2), 279–285. <https://doi.org/10.1016/j.jneumeth.2008.06.024>.
- (18) Andersen, R. A.; Musallam, S.; Pesaran, B. Selecting the Signals for a Brain–Machine Interface. *Curr. Opin. Neurobiol.* **2004**, 14 (6), 720–726. <https://doi.org/10.1016/j.conb.2004.10.005>.
- (19) Kostarelos, K.; Vincent, M.; Hebert, C.; Garrido, J. A. Graphene in the Design and Engineering of Next-Generation Neural Interfaces. *Adv. Mater.* **2017**, 29 (42), 1700909. <https://doi.org/10.1002/adma.201700909>.
- (20) Obien, M. E. J.; Deligkaris, K.; Bullmann, T.; Bakkum, D. J.; Frey, U. Revealing Neuronal Function through Microelectrode Array Recordings. *Frontiers in Neuroscience*. Frontiers Media S.A. 2015, p 423. <https://doi.org/10.3389/fnins.2014.00423>.
- (21) Lee, W.; Kim, D.; Rivnay, J.; Matsuhisa, N.; Lonjaret, T.; Yokota, T.; Yawo, H.; Sekino, M.; Malliaras, G. G.; Someya, T. Integration of Organic Electrochemical and Field-Effect Transistors for Ultraflexible, High Temporal Resolution Electrophysiology Arrays. *Adv. Mater.* **2016**, 28 (44), 9722–9728. <https://doi.org/10.1002/adma.201602237>.
- (22) Viventi, J.; Kim, D.-H.; Vigeland, L.; Frechette, E. S.; Blanco, J. A.; Kim, Y.-S.; Avrin, A. E.; Tiruvadi, V. R.; Hwang, S.-W.; Vanleer, A. C.; et al. Flexible, Foldable, Actively Multiplexed, High-Density Electrode Array for Mapping Brain Activity in Vivo. *Nat.*



- Neurosci.* **2011**, *14* (12), 1599–1605. <https://doi.org/10.1038/nn.2973>.
- (23) Hébert, C.; Masvidal-Codina, E.; Suarez-Perez, A.; Calia, A. B.; Piret, G.; Garcia-Cortadella, R.; Illa, X.; Del Corro Garcia, E.; De la Cruz Sanchez, J. M.; Casals, D. V.; et al. Flexible Graphene Solution-Gated Field-Effect Transistors: Efficient Transducers for Micro-Electrocorticography. *Adv. Funct. Mater.* **2017**, 1703976. <https://doi.org/10.1002/adfm.201703976>.
- (24) Blaschke, B. M.; Tort-Colet, N.; Guimerà-Brunet, A.; Weinert, J.; Rousseau, L.; Heimann, A.; Drieschner, S.; Kempinski, O.; Villa, R.; Sanchez-Vives, M. V.; et al. Mapping Brain Activity with Flexible Graphene Micro-Transistors. *2D Mater.* **2017**, *4* (2), 025040. <https://doi.org/10.1088/2053-1583/aa5eff>.
- (25) Hess, L. H.; Seifert, M.; Garrido, J. A. Graphene Transistors for Bioelectronics. **2013**. <https://doi.org/10.1109/JPROC.2013.2261031>.
- (26) Masvidal-Codina, E.; Illa, X.; Dasilva, M.; Calia, A. B.; Dragojević, T.; Vidal-Rosas, E. E.; Prats-Alfonso, E.; Martínez-Aguilar, J.; De la Cruz, J. M.; Garcia-Cortadella, R.; et al. High-Resolution Mapping of Infralow Cortical Brain Activity Enabled by Graphene Microtransistors. *Nat. Mater.* **2019**, *18* (3), 280–288. <https://doi.org/10.1038/s41563-018-0249-4>.
- (27) Drieschner, S.; Guimerà, A.; Cortadella, R. G.; Viana, D.; Makrygiannis, E.; Blaschke, B. M.; Vieten, J.; Garrido, J. A. Frequency Response of Electrolyte-Gated Graphene Electrodes and Transistors. *J. Phys. D: Appl. Phys.* **2017**, *50* (9), 095304. <https://doi.org/10.1088/1361-6463/aa5443>.
- (28) Mackin, C.; Hess, L. H.; Hsu, A.; Song, Y.; Kong, J.; Garrido, J. A.; Palacios, T. A Current–Voltage Model for Graphene Electrolyte-Gated Field-Effect Transistors. *IEEE Trans.*

- Electron Devices* **2014**, *61* (12), 3971–3977. <https://doi.org/10.1109/TED.2014.2360660>.
- (29) Rivnay, J.; Inal, S.; Salleo, A.; Owens, R. M.; Berggren, M.; Malliaras, G. G. Organic Electrochemical Transistors. *Nature Reviews Materials*. Nature Publishing Group January 16, 2018. <https://doi.org/10.1038/natrevmats.2017.86>.
- (30) Viventi, J.; Kim, D.-H.; Vigeland, L.; Frechette, E. S.; Blanco, J. A.; Kim, Y.-S.; Avrin, A. E.; Tiruvadi, V. R.; Hwang, S.-W.; Vanleer, A. C.; et al. Flexible, Foldable, Actively Multiplexed, High-Density Electrode Array for Mapping Brain Activity in Vivo. *Nat. Neurosci.* **2011**, *14* (12), 1599–1605. <https://doi.org/10.1038/nn.2973>.
- (31) Chaparro, L. Fourier Analysis in Communications and Filtering. In *Signals and Systems Using MATLAB*; Elsevier, 2015; pp 449–490. <https://doi.org/10.1016/b978-0-12-394812-0.00007-3>.
- (32) Cisneros-Fernandez, J.; Dei, M.; Teres, L.; Serra-Graells, F. Switch-Less Frequency-Domain Multiplexing of GFET Sensors and Low-Power CMOS Frontend for 1024-Channel MEGCoG. In *2019 IEEE International Symposium on Circuits and Systems (ISCAS)*; IEEE, 2019; pp 1–5. <https://doi.org/10.1109/ISCAS.2019.8702544>.
- (33) Hébert, C.; Masvidal-Codina, E.; Suarez-Perez, A.; Calia, A. B.; Piret, G.; Garcia-Cortadella, R.; Illa, X.; Del Corro Garcia, E.; De la Cruz Sanchez, J. M.; Casals, D. V.; et al. Flexible Graphene Solution-Gated Field-Effect Transistors: Efficient Transducers for Micro-Electrocorticography. *Adv. Funct. Mater.* **2018**, *28* (12), 1703976. <https://doi.org/10.1002/adfm.201703976>.
- (34) Dreier, J. P.; Reiffurth, C. The Stroke-Migraine Depolarization Continuum. *Neuron* **2015**, *86* (4), 902–922. <https://doi.org/10.1016/j.neuron.2015.04.004>.
- (35) Lauritzen, M.; Dreier, J. P.; Fabricius, M.; Hartings, J. A.; Graf, R.; Strong, A. J. Clinical

- Relevance of Cortical Spreading Depression in Neurological Disorders: Migraine, Malignant Stroke, Subarachnoid and Intracranial Hemorrhage, and Traumatic Brain Injury. *J. Cereb. Blood Flow Metab.* **2011**, *31* (1), 17–35. <https://doi.org/10.1038/jcbfm.2010.191>.
- (36) Fang, H.; Yu, K. J.; Gloschat, C.; Yang, Z.; Song, E.; Chiang, C.-H.; Zhao, J.; Won, S. M.; Xu, S.; Trumpis, M.; et al. Capacitively Coupled Arrays of Multiplexed Flexible Silicon Transistors for Long-Term Cardiac Electrophysiology. *Nat. Biomed. Eng.* **2017**, *1* (3), 0038. <https://doi.org/10.1038/s41551-017-0038>.